Chapter 1

XAI for Wireless Communications

Abdul-Karim Gizzini[a], Yahia Medjahdi[b], Ali J. Ghandour[c], Laurent Clavier[b], and Mouna Ben Mabrouk[a]

[a]SogetiLabs Research and Innovation (part of Capgemini), Issy Les Moulineaux, France, [b]IMT Nord Europe, Institut Mines Télécom, Centre for Digital Systems, Villeneuve d'Ascq, France, [c]National Center for Remote Sensing, CNRS, Mansourieh, Lebanon

ABSTRACT

The native artificial intelligence (AI) concept is envisioned to be integrated into 6G future communications. Due to the black-box nature of the majority of AI models, the decision-making strategy used by these models is critical, risky, and challenging. This issue can be tackled by developing explainable AI (XAI) schemes that aim to explain the logic behind the black-box model behavior, and thus, ensure its efficient and safe deployment. In this context, this chapter highlights the main challenges of the recent AI-based solutions for wireless communications, in particular, physical (PHY) layer applications. In addition to that, the latest research efforts toward designing XAI schemes for PHY layer applications are discussed. As a case study, this chapter presents an XAI-based scheme for channel estimation in wireless communications, where the presented scheme shows that employing XAI can offer a bunch of advantages including (1) understanding the black-box model behavior, (2) reducing the overall computational complexity of the employed AI model, and (3) improving the performance of the desired application. Finally, a list of future research directions is provided.

KEYWORDS

6G, Wireless communications, AI, XAI, Physical layer, Channel estimation

1.1 INTRODUCTION

Artificial intelligence (AI) is expected to play a crucial role in the overall design of future 6G networks [34, 4]. In particular, native (AI) will be embedded within the functionality of all layers [24] to support demands for high data rates and low latency-critical applications. According to [36], the AI-enabled intelligent architecture for 6G networks defines several layers, including the intelligent sensing layer, where accurate environment monitoring is critical for 6G smart applications like autonomous driving [3]. Consequently, a robust physical (PHY) layer design is needed to ensure the reliability of the intelligent sensing layer.

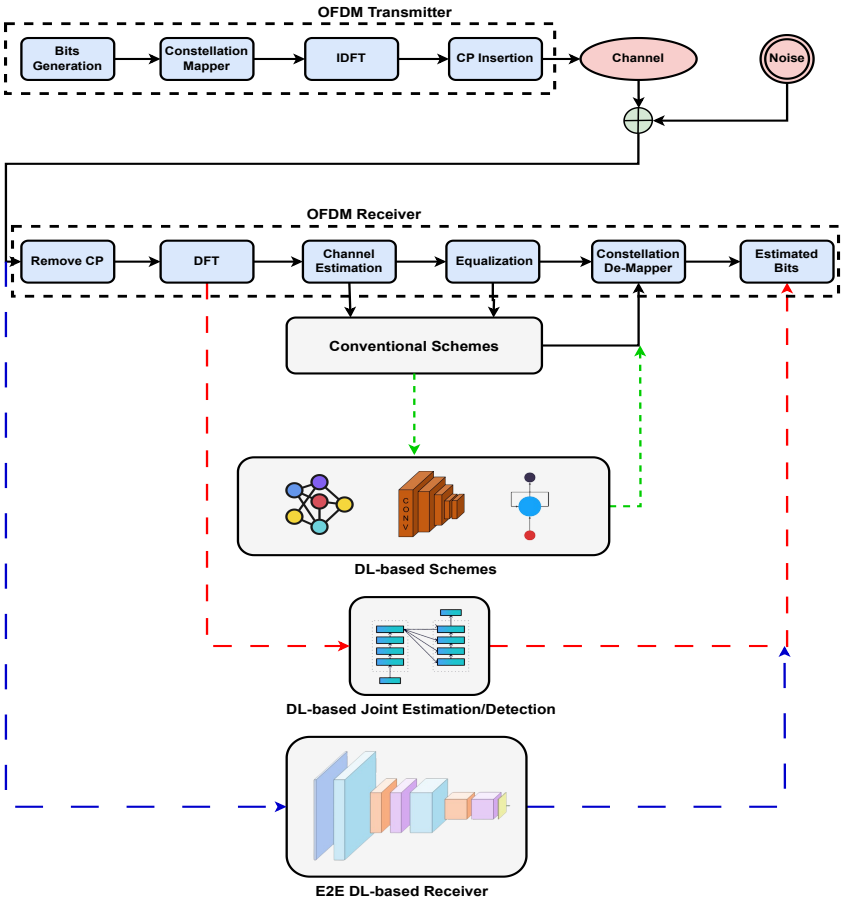

FIGURE 1.1 AI-based PHY layer applications.

Recently, deep learning (DL) has been employed in the PHY layer of wireless communications, in particular within the receiver design [20, 29], including signal classification and detection [30, 28, 8], channel estimation [18, 11], joint channel estimation and equalization [31], and end-to-end (E2E) DL-based receiver design [19, 41, 2, 7, 16]. These DL-based solutions have been integrated into PHY layer applications to provide better performance-complexity trade-offs and robustness than conventional schemes. Figure 1.1 summarizes the employment of different DL networks within the orthogonal frequency division multiplexing (OFDM) receiver design. Among these DL networks, feed-forward neural network (FNN), convolutional neural network (CNN), and recurrent neural network (RNN) have been employed in the channel estimation task [11], where the objective is to use the DL network as denoising until after conventional

estimated channel. Moreover, DL networks can learn the time and frequency collection of the wireless channel, hence providing good performance compared to conventional channel estimation schemes. Moreover, signal detection application has been studied in [8, 30, 28] where CNN and transformers have been employed to classify the received symbols from the received frequency domain signal.

Apart from single-task DL-based solutions, joint channel estimation, and equalization in addition to the detection have been studied in [19, 31]. In this context, the authors in [31] have proposed an efficient transformer-based scheme called SigT to detect the received bits from the received frequency domain signal. Moreover, an ablation study is performed to select the best model architecture. This ablation study is based on removing some layers, i.e., convolutional, pooling, dropout, etc., and measuring the train and test accuracy of the proposed architecture. Finally, the architecture corresponding to the highest training and testing accuracies is chosen. A similar objective has been studied in [19] where the DeepRx receiver is proposed to estimate the received bits from the received frequency domain signal, the received pilots, and the channel response.

A vast of research works have focused on the E2E DL-based receiver design [16]. We note that such design consists of implementing a transmitter, channel, and receiver as a single DL black-box network referred to as an autoencoder, as shown in Figure 1.1. In [38] a neural receiver consisting of dense layers has been proposed to predict the transmitted bits based on jointly processing the received OFDM symbols. In this work, the while receiver is considered as a black-box DL model. Another work has been proposed in [2], where a convolutional residual neural network is used to predict the log-likelihood ratios (LLRs) of the received bits taking the received signal. After that, the predicted LLRs are fed to the channel decoder after a deinterleaving step to detect the final received bits. A multiuser multiple-input multiple-output (MU-MIMO) receiver with 5G New Radio (5G NR) has been proposed in [7], where consecutive CNN layers are used to exploit the time and frequency correlation of the channel, in addition to a graph neural network (GNN) to handle multiple users. The proposed receiver takes the received post-FFT signal, the positional encoded pilot distance, in addition to optionally fed the noise power and the estimated channel matrix within the inputs. We note that the discussed E2E DL-based receivers employ real-valued DL networks, however, a complex-valued DL-based OFDM receiver has been proposed in [41] where two CNN networks are proposed to work within a 2-stage operations. The first network performs channel estimation and equalization, and the second is dedicated to the received bits detection. Similar to the work accomplished in [31], an ablation study is performed using 6 different CNN structures to select the best architecture to be employed. It is worth mentioning that regardless of the good performance offered by different E2E DL-based receivers in comparison to the conventional receivers, still the intuition behind selecting the model inputs and architecture is empirically

Application	Reference	DL Model		
		Architecture	Inputs	Output
Channel Estimation	[11]	FNN, RNN, CNN	Conventional estimated channel	Denoised estimated channel
Signal Detection	[8]	CNN	Received frequency domain signal Channel resposne	Demodulated symbols
	[29]	CNN	Received frequency domain signal	
	[27]	Transformer	Received frequency domain signal	
Joint Estimation Equalization Detection	[30]	Transformer	Received frequency domain signal	Received bits
	[18]	CNN	Received frequency domain signal Received pilots Channel response	
E2E DL-based Receiver	[40]	DCCN	Received time domain signal	LLRs
	[2]	CNN + ResNet	Received time domain signal	
	[7]	CNN + FNN	Received frequency domain signal Encoded pilot distance Noise power	
	[15]	CNN + ResNet	Received frequency domain signal	

TABLE 1.1 DL-based PHY layer applications (the list is not exhaustive).

performed. Therefore, it is not possible to efficiently optimize the DL-based solutions. Table 1.1 summarizes the surveyed DL-based solution for different PHY layer applications.

1.2 TOWARD XAI-BASED SOUTIONS

The DL-based PHY layer solutions encounter three main concerns:

- High computational complexity: High-complex DL architectures are employed to guarantee good performance. However, this is impractical in IoT and low-latency critical applications such as autonomous driving. Therefore, reducing the computational complexity while preserving or improving the overall system performance is challenging.
- Identifying the relevant inputs: filtering the most important DL model inputs is crucial for optimizing its performance. Knowing that the majority of DL-

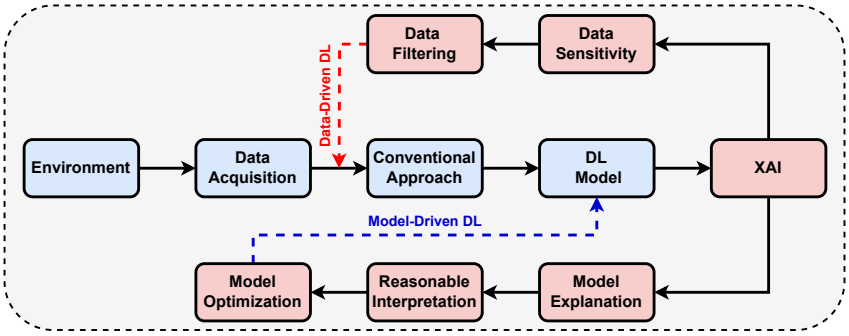

FIGURE 1.2 The XAI-based long-term evolution of the PHY layer Design. [40]

based solutions use an empirical input selection strategy, finding a smart input filtering strategy is necessary to optimize the system's performance.

- Trustworthy deployment: The majority of the utilized DL models are black-box models. Consequently, researchers and industrial leaders are not able to trust the employment of these models in real-case sensitive applications [22].

It is worth mentioning that the discussed concerns are mainly due to the black-box nature of the utilized DL models, which in turn prevents researchers from understanding the logic behind the decision-making strategy of these models. Therefore, designing XAI-based solutions enables safe efficient, and robust AI employment in real-case scenarios. Figure 1.2 illustrates the main advantages of integrating the XAI schemes into the PHY layer design. As we can notice, the XAI post-processing of the DL black-box offers two main advantages listed below:

- Smart data-driven DL-based solution: Employing XAI schemes allows the smart identification of the model inputs, hence the collected data from the environment can be filtered accordingly. Therefore the employed DL model can focus on the main relevant inputs to improve its performance. Moreover, it has been shown in [15] that considering the whole received data as an input to the model degrades the model performance since additional irrelevant inputs can be considered as noise and thus it is essential to filter them before employing the DL processing.
- Efficient model-driven DL-based solution: Another key advantage in the XAI integration within the PHY layer lies in providing internal interpretability of the employed black-box model. Consequently, it is possible to assign neuron-level relevance scores for the employed model architecture. Therefore, optimizing the model architecture by removing the irrelevant neurons will reduce the overall computational complexity while preserving the model's performance in addition to providing a clear and reasonable interpretation of the model behavior.

The majority of XAI-related works in the literature are surveys and reviews about the guidelines and importance of using XAI in wireless communications. The main definitions, concepts, and taxonomy of XAI are discussed in [17]. A Novel Knowledge-powered framework for network automation that effectively adapts to the dynamic changes of complex communication systems has been proposed in [35]. The authors in [6] provide a comprehensive survey on the use of explainable artificial intelligence (XAI) to design a trustworthy explainable open radio access network (O-RAN) architecture. In addition to that, Shapley additive explanations (SHAP) XAI scheme has been employed to assign the importance of the features within the context of the Streamlined Automation-Native 6G Networks [25]. SHAP XAI scheme has been also employed for energy-efficient resource allocation [5, 27, 23], where it assigns importance to the features used by the deep reinforcement learning (DRL) agent at each state. These features could be the utilized bandwidth, number of active antennas, number of connected users, and the average data rate. XAI has been employed in the internet-of-things (IoT) networks [21], where the authors in [42] have proposed a novel model-agnostic XAI scheme denoted as transparency relying upon statistical theory (TRUST) for numerical applications. The TRUST scheme is oriented toward cybersecurity of the industrial IoT (IIoT), where it outperforms the local interpretable model-agnostic explanations (LIME) scheme [32] in terms of performance, speed, and explainability.

Knowing that the recent XAI schemes focus mainly on network optimization, resource allocation, and secure IoT. Hence, they can not be adapted to the PHY layer applications since such applications lack clear discriminative features within the model inputs. Therefore, this chapter aims to highlight the recent advances in employing XAI schemes for PHY layer applications in wireless communications, specifically, channel estimation [15]. We note that channel estimation here is just a case study and the discussed XAI scheme could be easily adapted to any other PHY layer application.

1.3 SIGNAL MODEL

This section presents the considered system model in this chapter based on the IEEE 802.11p standard [1]. Let $\boldsymbol{s}_i \in \mathbb{C}^{K\times 1}$ denotes the i-th transmitted frequency-domain OFDM symbol that can be expressed as:

$$\boldsymbol{s}_i[k] = \begin{cases} \boldsymbol{s}_{i,d}[k], & k \in \{K\}_{\mathrm{d}} \\ \boldsymbol{s}_{i,p}[k], & k \in \{K\}_{\mathrm{p}} \\ 0, & k \in \{K\}_{\mathrm{n}} \end{cases} \tag{1.1}$$

where $0 \leq k \leq K-1$ denotes the subcarrier index. We note that K_{on} useful subcarriers are used where $K_{\mathrm{on}} = K_p + K_d$. $\boldsymbol{s}_{i,p} \in \mathbb{C}^{K_p\times 1}$ and $\boldsymbol{s}_{i,d} \in \mathbb{C}^{K_d\times 1}$ represent the allocated pilot symbols and the modulated data symbols at a set of subcarriers denoted $\{K\}_{\mathrm{p}}$ and $\{K\}_{\mathrm{d}}$, respectively. $K_n = K - K_{\mathrm{on}}$ denotes the

null guard band subcarriers. K_{cp} samples are added to the time-domain OFDM symbol resulting in $\boldsymbol{x}_i \in \mathbb{C}^{K+K_{\text{cp}}\times 1}$.

The i-th received frequency-domain OFDM symbol $\boldsymbol{y}_i \in \mathbb{C}^{K_{\text{on}}\times 1}$ is expressed as follows:

$$\boldsymbol{y}_i[k] = \boldsymbol{h}_i[k]\boldsymbol{s}_i[k] + \boldsymbol{e}_i[k] + \tilde{\boldsymbol{v}}_i[k], \tag{1.2}$$

$\boldsymbol{h}_i \in \mathbb{C}^{K_{\text{on}}\times 1}$, $\tilde{\boldsymbol{v}}_i \in \mathbb{C}^{K_{\text{on}}\times 1}$, and $\boldsymbol{e}_i \in \mathbb{C}^{K_{\text{on}}\times 1}$ refer to the frequency-time response of the doubly-selective channel, the additive white Gaussian noise (AWGN) at the i-th OFDM, and the Doppler-induced inter-carrier interference derived in [12], respectively. $\boldsymbol{e}_i$ can be expressed as:

$$\boldsymbol{e}_i[k] = \frac{1}{K}\sum_{\substack{q=0\\ q\neq k}}^{K-1}\sum_{n=0}^{K-1}\boldsymbol{h}_i[q,n]e^{-j2\pi\frac{n(k-q)}{K}}\boldsymbol{s}_i[q]. \tag{1.3}$$

1.4 FNN-BASED CHANNEL ESTIMATION SCHEMES

Among different OFDM receiver operations, the accuracy of the channel estimation highly impacts the overall performance and reliability of the OFDM receiver. This is because a precisely estimated channel influences the follow-up equalization and decoding operations at the receiver [11]. In this context, channel estimation is the first challenging task within the OFDM receiver chain due to the nature of the wireless channel especially in mobile applications where the channel is doubly selective. We note that in a mobile wireless environment, transmitted signals propagate through many paths with different attenuations, delays, and Doppler shifts resulting from the motion of network nodes within the surrounding environment. As a result, the wireless channel becomes frequency-selective and time-varying which defines its doubly selective nature.

FNN networks have been widely used in literature as a post-processing unit added to some initial channel estimation due to their low computational complexity compared to other DL networks such as CNNs and RNNs. Similarly to the other DL-based PHY layer solutions, FNN-based channel estimation schemes can achieve good performance. Still, the logic behind choosing the FNN architecture, i.e., the number of hidden layers and neurons as well as the suitable FNN inputs is unclear. We note that the majority of the FNN-based channel estimation schemes use a 3 hidden layer FNN architecture with different configurations. In [26], an FNN-based scheme has been proposed where the FNN takes the received signal, received pilots, and previously estimated channel to predict the current channel estimates. The utilized FNN architecture consists of 3 hidden layers with 500, 250, and 120 neurons, respectively. Simulation results show that using this FNN input combination improves performance. Another FNN-based channel estimation scheme has been proposed in [37] where the

Reference	DL Model	
	Architecture	Inputs
[35]	512-256-128	$\hat{\boldsymbol{h}}_{\text{LS}_i}$, $\hat{\boldsymbol{h}}_{\text{FNN}_{i-1}}$
[25]	500-250-120	$\boldsymbol{y}_i, \boldsymbol{s}_{i,p}, \hat{\boldsymbol{h}}_{\text{FNN}_{i-1}}$
[17]	40-20-40	$\hat{\boldsymbol{h}}_{\text{DPA}_i}$
[10]	15-15-15	$\hat{\boldsymbol{h}}_{\text{STA}_i}$
[13]	15-15-15	$\hat{\boldsymbol{h}}_{\text{TRFI}_i}$

TABLE 1.2 FNN-based channel estimation schemes (the list is not exhaustive).

least squares (LS) estimated channel combined with the previously estimated channel are fed as an input to a 3 hidden layer FNN consisting of 512, 256, and 128 neurons, respectively. Employing LS as an FNN input improves the channel estimation accuracy and provides comparable performance to the linear minimum mean square error (LMMSE) channel estimation scheme.

Recently, the authors in [11] show that improving the conventional channel estimation accuracy allows the employment of low-complex FNN architectures. In [18], the authors proposed an FNN-based channel estimation scheme that applies data-pilot aided (DPA) channel estimation prior to a 3 hidden layer FNN consisting of 40, 20, and 40 neurons, respectively. Similarly, in [10] and [14] the authors used a 3 hidden layer FNN architecture with 15 neurons per layer on top of the conventional spectral temporal averaging (STA) [9] and time-domain reliable test frequency domain interpolation (TRFI) [39] channel estimation schemes. This computational complexity reduction is motivated by the fact that the conventional STA and TRFI channel estimation schemes outperform the DPA channel estimation. Hence, STA-FNN and TRFI-FNN outperform the DPA-FNN [18] while recording a substantial computational complexity decrease. Table 1.2 summarizes the discussed FNN-based channel estimation schemes. In the following, we present the channel estimation steps employed mainly by the STA-FNN, and TRFI-FNN channel estimation schemes.

1.4.1 STA-FNN

The STA-FNN [10] channel estimation is based on the DPA estimation that aims to track the doubly selective channel variations by using the received demapped data subcarriers of the previously received symbols. These demapped subcarriers are then used to estimate the channel for the existing symbol such that

$$\boldsymbol{d}_i[k] = \mathfrak{D}\big(\frac{\boldsymbol{y}_i[k]}{\hat{\boldsymbol{h}}_{\text{DPA}_{i-1}}[k]}\big),\ \hat{\boldsymbol{h}}_{\text{DPA}_0}[k] = \hat{\boldsymbol{h}}_{\text{LS}}[k], \tag{1.4}$$

where $\mathfrak{D}(.)$ refers to the demapping operation to the nearest constellation point following the employed modulation order. $\hat{\boldsymbol{h}}_{\mathrm{LS}}$ signifies the LS estimated channel at the received preambles, such that

$$\hat{\boldsymbol{h}}_{\mathrm{LS}}[k] = \frac{\sum_{u=1}^{P} \boldsymbol{y}_u^{(p)}[k]}{P\boldsymbol{\Lambda}[k]},\ k \in \{K\}_{\mathrm{on}}\,, \tag{1.5}$$

where $\boldsymbol{\Lambda}$ denotes the frequency domain predefined preamble sequence. After that, the final DPA channel estimates are updated in the following manner

$$\hat{\boldsymbol{h}}_{\mathrm{DPA}_i}[k] = \frac{\boldsymbol{y}_i[k]}{\boldsymbol{d}_i[k]}. \tag{1.6}$$

Finally, frequency and time-domain averaging are applied on top of the DPA estimated channel as proposed in the STA channel estimation scheme [9] where

$$\hat{\boldsymbol{h}}_{\mathrm{FD}_i}[k] = \sum_{\lambda=-\beta}^{\lambda=\beta} \omega_\lambda \hat{\boldsymbol{h}}_{\mathrm{DPA}_i}[k+\lambda],\ \omega_\lambda = \frac{1}{2\beta+1}. \tag{1.7}$$

$$\hat{\boldsymbol{h}}_{\mathrm{STA}_i}[k] = (1-\frac{1}{\alpha})\hat{\boldsymbol{h}}_{\mathrm{STA}_{i-1}}[k] + \frac{1}{\alpha}\hat{\boldsymbol{h}}_{\mathrm{FD}_i}[k]. \tag{1.8}$$

FNN is utilized as a post-processing unit after the conventional STA scheme [10]. STA-FNN captures more the time-frequency correlations of the channel samples, apart from correcting the conventional STA estimation error. Furthermore, the STA-FNN channel estimation scheme records an error floor in a high SNR region. This limitation arises from fixing the frequency and time-averaging coefficients in the conventional STA channel estimation. Consequently, the final STA estimated channel is considered as a linear combination between $\hat{\boldsymbol{h}}_{\mathrm{STA}_{i-1}}[k]$ (1.8) and $\hat{\boldsymbol{h}}_{\mathrm{FD}_i}$ (1.7). However, this linear combination is not always valid, especially in real-case scenarios due to the doubly selective nature of the wireless channel.

1.4.2 TRFI-FNN

To further improve the performance in high SNR regions, TRFI-FNN has been proposed [14] where the same FNN architecture as in [10] is integrated with the conventional TRFI channel estimation [39]. We note that TRFI divided the received subcarriers into reliable RS_i and unreliable subcarriers URS_i, where cubic interpolation is used to estimate the channel for the unreliable subcarriers. This procedure can be expressed in the following manner

- Equalize the previously received OFDM symbol by $\hat{\boldsymbol{h}}_{\mathrm{TRFI}_{i-1}}[k]$ and $\hat{\boldsymbol{h}}_{\mathrm{DPA}_i}[k]$, such that

$$\boldsymbol{d'}_{i-1}[k] = \mathfrak{D}\big(\frac{\boldsymbol{y}_{i-1}[k]}{\hat{\boldsymbol{h}}_{\mathrm{DPA}_i}[k]}\big),\ \boldsymbol{d''}_{i-1}[k] = \mathfrak{D}\big(\frac{\boldsymbol{y}_{i-1}[k]}{\hat{\boldsymbol{h}}_{\mathrm{TRFI}_{i-1}}[k]}\big). \tag{1.9}$$

- According to the demapping results, the subcarriers are divided into RS_i and URS_i as follows

$$\begin{cases} RS_i \leftarrow RS_i + k, & \boldsymbol{d'}_{i-1}[k] = \boldsymbol{d''}_{i-1}[k] \\ URS_i \leftarrow URS_i + k, & \boldsymbol{d'}_{i-1}[k] \neq \boldsymbol{d''}_{i-1}[k] \end{cases}. \tag{1.10}$$

- As a final step, frequency-domain cubic interpolation is employed to estimate the channels at the URS_i as follows

$$\hat{\boldsymbol{h}}_{\mathrm{TRFI}_i}[k] = \begin{cases} \hat{\boldsymbol{h}}_{\mathrm{DPA}_i}[k], & k \in RS_i \\ \text{Cubic Interpolation}, & k \in URS_i \end{cases}. \tag{1.11}$$

We note that frequency-domain interpolation enhances the performance. However, the main drawback of the TRFI channel estimation lies in the strategy used to divide the RS_i and URS_i subcarriers. Since the condition where $\tilde{\boldsymbol{d}}'_{i-1}[k] \neq \tilde{\boldsymbol{d}}''_{i-1}[k]$ is more dominant in high mobility scenarios. Hence, the number of selected RS_i becomes limited thus degrading the performance of the employed cubic interpolation.

1.5 XAI FOR CHANNEL ESTIMATION

The authors in [15] proposed a perturbation-based model-agnostic global XAI scheme called XAI-CHEST which jointly performs the channel estimation task as well as provides the corresponding reasonable explanations. XAI-CHEST scheme consists mainly of two concatenated FNN models called the interpretability model N and the utility model U, respectively. The U model corresponds to the black-box FNN model which is responsible for doing the channel estimation task taking as an input the conventional estimated channel $\hat{\tilde{\boldsymbol{h}}}'_{\Phi_i} \in \mathbb{R}^{2K_{\mathrm{on}} \times 1}$, where $\Phi \in [\mathrm{STA}, \mathrm{TRFI}]$. we note that the U model is trained prior to the integration of the N model. Hence, the weights of the U model denoted as θ_U are considered to be frozen while the training of the N model.

The key idea of the XAI-CHEST scheme lies in the functionality of the N model, which is trained to produce a noise-weight mask $\boldsymbol{b}'_{\Phi_i}$ that highlights the importance of the conventional estimated channel vector $\hat{\tilde{\boldsymbol{h}}}'_{\Phi_i}$. High $\boldsymbol{b}'_{\Phi_i}[k]$ signifies that the corresponding subcarrier is irrelevant and thus it could be discarded from $\hat{\tilde{\boldsymbol{h}}}'_{\Phi_i}$. In contrast, low $\boldsymbol{b}'_{\Phi_i}[k]$ reveal the importance of including the corresponding subcarrier within $\hat{\tilde{\boldsymbol{h}}}'_{\Phi_i}$. We note that generating $\boldsymbol{b}'_{\Phi_i}$ is subject to preserving the performance of the initially pre-trained U model while feeding the noisy conventional estimated channel as an input to the U model. The whole process of the XAI-CHEST is summarized as follows:

1. training the U model with $\hat{\tilde{\boldsymbol{h}}}'_{\Phi_i}$ as an input and save the U model weights θ_U.

2. Generate the noise weight mask $\boldsymbol{b}'_{\Phi_i}$ by the N model with $\hat{\tilde{\boldsymbol{h}}}'_{\Phi_i}$ as an input.

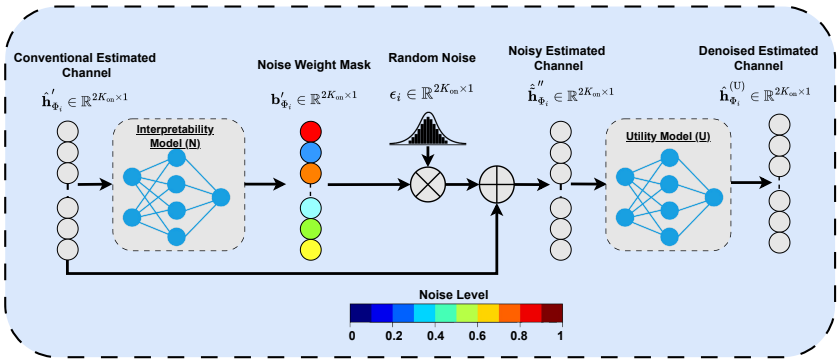

FIGURE 1.3 Perturbation-based XAI-CHEST scheme.

3. Multiply the generated noise mask $\boldsymbol{b}'_{\Phi_i}$ by a random noise.
4. Generate a noisy conventional estimated channel $\hat{\tilde{\boldsymbol{h}}}''_{\Phi_i}$ by adding the weighted noise from step 3 to the conventional estimated channel.
5. Fed $\hat{\tilde{\boldsymbol{h}}}''_{\Phi_i}$ as an input to the pre-trained U model and measure the mean squared error (MSE) loss.
6. Update the N model weights θ_N by minimizing the customized loss between the MSE obtained in step 5 and the generated noise weight mask from step 2. As a result, the N model is trained in order to minimize the MSE loss of the U model taking into consideration the added noise.

The XAI-CHEST scheme allows the N model to induce noise on the U model inputs without degrading its performance. hence, the N model will only induce high noise on the inputs that are not substantial to the U model's proper functioning. Based on the generated noise mask by the N model, the U model inputs can be classified as either relevant or irrelevant inputs, where re-training the U model taking only the relevant subcarriers leads to a significant performance improvement. Moreover, the explanations offered by the U model can be exploited to reduce its computational complexity cost. Figure 1.3 illustrates the full process performed by the XAI-CHEST scheme. We note that more technical details can be found in [15].

1.6 PERFORMANCE EVALUATION

This section illustrates the performance evaluation of the studied XAI scheme. We note that based on the obtained XAI results, the inputs of the studied FNN-based channel estimation schemes are divided into relevant, and irrelevant subcarriers. After that, the bit error rate (BER) performance is analyzed considering each configuration, where the impact of the conventional channel estimation on the obtained XAI results is discussed.

TABLE 1.3 Characteristics of the employed channel models.

Channel model	Average path gains [dB]	Path delays [ns]
VTV-EX	[0, 0, 0, -6.3, -6.3, -25.1, -25.1, -25.1, -22.7, -2.27, -22.7]	[0, 1, 2, 100, 101, 200, 201, 202, 300, 301, 302]
VTV-SDWW	[0, 0, -11.2, -11.2, -19, -21.9, -25.3, -25.3, -24.4,-28, -26.1, -26.1]	[0, 1, 100, 101, 200, 300, 400, 401, 500, 600, 700, 701]

1.6.1 Simulation Setup

The performance evaluation aims to study the impact of conventional channel estimation on the provided explanations obtained by the studied XAI scheme. In this context, we consider two channel models [33]: (*i*) Low-frequency selectivity (LFS), where VTV Expressway (VTV-EX) scenario is employed. (*ii*) High-frequency selectivity (HFS), where VTV Expressway Same Direction with Wall (VTV-SDWW) scenario is considered, as shown in Table 1.3. In both scenarios, Doppler frequency $f_d = 1000$ Hz, and QPSK modulation is considered. Both the U and N models are trained using a 100, 000 OFDM symbols dataset, splitted into 80% training, and 20% testing. ADAM optimizer is used with a learning rate $lr = 0.001$ with batch size equals 128 for 500 epoch. Simulation parameters are based on the IEEE 802.11p standard [11], where the comb pilot allocation is used so that $K_p = 4$, $K_d = 48$, $K_n = 12$, and $I = 50$. Table 1.4 summarizes the simulation parameters considered in this work.

TABLE 1.4 Parameters of the studied FNN-based channel estimation schemes.

Parameter	Values
FNN (Hidden layers; Neurons per layer)	(3;15-15-15)
Activation function	ReLU
Number of epochs	500
Training samples	800000
Testing samples	200000
Batch size	128
Optimizer	ADAM
Loss function	MSE
Learning rate	0.001
Training SNR	40 dB

1.6.2 BER Performance Analysis

To illustrate the efficiency of the XAI-CHEST scheme, we first simulate the BER performance considering several combinations of different relevant and irrelevant subcarriers. These combinations are generated based on the generated

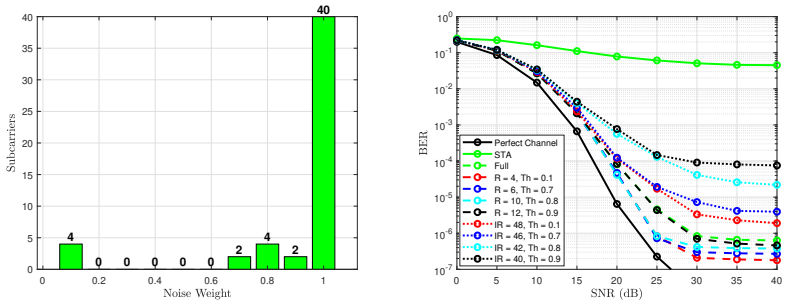

(a) Noise weight distribution. (b) BER performance.

FIGURE 1.4 BER performance of relevant and irrelevant subcarriers employing the STA-FNN channel estimation scheme and the LFS channel model.

noise mask by the N model shown in Figure 1.4(a). For simplicity, we used the LFS channel model with the STA-FNN channel estimation scheme. As we can notice the distribution is shifted towards one, where most subcarriers are assigned noise weight equal to one. This signifies that in simple scenarios like the LFS channel model, the STA-FNN model ignores the majority of the subcarriers to refine the conventional STA estimated channel. A nice observation is that the pilot subcarriers are assigned the lowest noise weight, i.e., 0.1. This reveals that the STA-FNN model cannot neglect the estimated channels at the pilots, and considering them is crucial for high estimation accuracy. This observation is further highlighted in Figure Figure 1.4(b), where we can notice that employing only the pilot subcarriers within the STA-FNN model input gives the best BER performance. Moreover, adding more relevant subcarriers to the pilots is not beneficial. Hence, considering only the pilots in the LFS channel model is enough, and there is no need to consider any other subcarriers. More details on selecting the optimal threshold to filter the relevant subcarriers are found in [13].

To study the impact of the initial channel estimation on the generated noise weights we considered both the STA-FNN and TRFI-FNN channel estimation schemes. We note that the TRFI-FNN outperforms the STA-FNN scheme in high SNR regions due to the employed cubic interpolation in the conventional TRFI channel estimation [11]. Hence, we expect that the TRFI-FNN scheme will require fewer relevant subscribers since we are training the N model on 40 dB SNR. This expectation is validated in both LFS and HFS channel models as shown in Figure 1.5. We can clearly notice from Figure 1.5(a) that the generated noise weights for the TRFI estimated channels are either relevant or irrelevant, i.e., the assigned noise weight is either 0.1 or 1. Hence, when the frequency selectivity of the channel is low, the pilot subcarriers are enough regardless of the employed initial channel estimation prior to the FNN model processing. The impact of the initial channel estimation is more dominant in the HFS channel

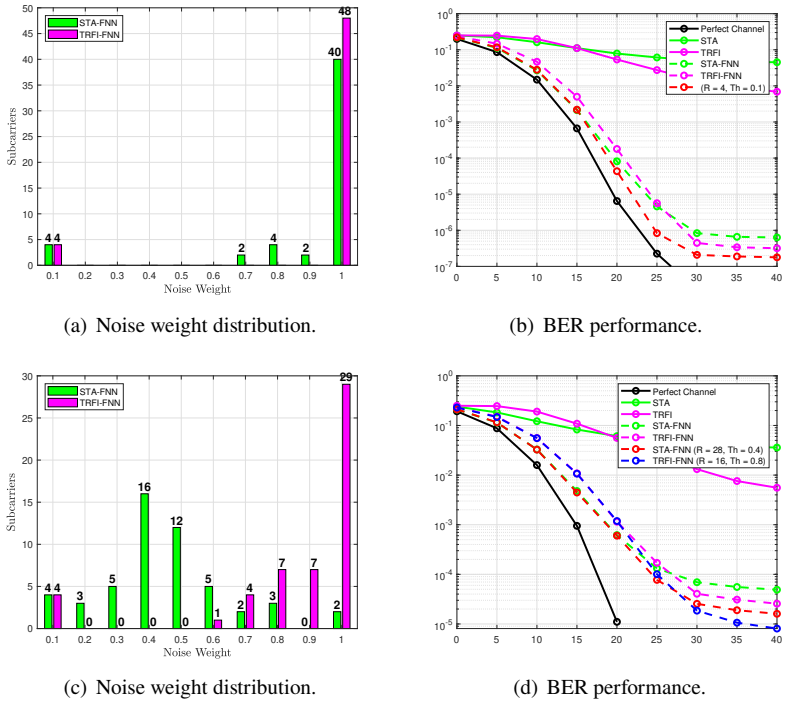

(a) Noise weight distribution. (b) BER performance.

(c) Noise weight distribution. (d) BER performance.

FIGURE 1.5 Performance evaluation of the studied STA-FNN and TRFI-FNN channel estimation schemes employing the LFS and HFS channel models.

estimation as we can notice in Figure 1.5(c), where the distribution of $\boldsymbol{b}'_{\text{STA}_i}$ is distributed towards zero signifying that the STA-FNN needs more relevant subcarriers in refining the STA estimated channel. On the contrary, $\boldsymbol{b}'_{\text{TRFI}_i}$ is still shifted towards one even though the scenario is more complicated compared to employing the LFS channel model. This is further validated in the BER simulations, Figure 1.5(d), where the TRFI-FNN model requires 16 relevant subcarriers, whereas, the STA-FNN model requires 28 relevant subcarriers to achieve the best possible performance. Therefore, we can conclude that as the accuracy of the initial channel estimation improves, fewer relevant subcarriers are required and vice-versa. Moreover, optimizing the inputs of the FNN model contributes to reducing the overall computational complexity as discussed in [13].

1.7 CONCLUSION

Designing trustworthy efficient AI-based solutions is critical in future 6G communications. This chapter highlighted the recent advances in the XAI-based schemes for physical layer applications, where channel estimation is considered

as a case study. First of all, different DL-based physical layer schemes have been surveyed, where the main challenges encountered in the practical implementation of such schemes are well-defined. After that, the long-term evolution of the XAI in the physical layer design is presented where smart data-driven and efficient model-driven solutions can be designed. A perturbation-based XAI scheme for channel estimation denoted as XAI-CHEST is then presented and tested on two recent FNN-based channel estimation schemes. XAI-CHEST scheme aims to filter the relevant model inputs by inducing high noise on the irrelevant inputs without harming the model's performance. Thus, enabling a trustworthy, optimized, and robust channel estimation. Simulation results reveal that employing only the relevant elements within the channel estimation leads to a significant improvement in the BER performance while optimizing the FNN input. Moreover, filtering the relevant inputs is highly related to the scenario, wherein the HFS channel, the FNN-based channel estimation model requires more relevant inputs in comparison to the LFS channel scenario. Finally, we concluded that improving the initial channel estimation prior to the FNN processing reduces the required relevant inputs needed to achieve the best possible performance. As a future perspective, the overall optimization of the DL model, i.e., selecting the relevant inputs as well as optimizing the model architecture simultaneously is an important research direction. Moreover, proposing gradient-based XAI schemes is crucial since such schemes provide better interpretability compared to perturbation-based schemes due to employing the internal model architecture in manipulating the relevance scores.

Bibliography

[1] Abdeldime Abdelgader and Lenan Wu. "The Physical Layer of the IEEE 802.11 p WAVE Communication Standard: The Specifications and Challenges". In: *The Physical Layer of the IEEE 802.11 p WAVE Communication Standard: The Specifications and Challenges*. Vol. 2. Oct. 2014.

[2] Fayçal Ait Aoudia and Jakob Hoydis. "End-to-end learning for OFDM: From neural receivers to pilotless communication". In: *IEEE Transactions on Wireless Communications* 21.2 (2021), pp. 1049–1063.

[3] M. I. Ashraf et al. "Towards Low-Latency and Ultra-Reliable Vehicle-to-Vehicle Communication". In: *2017 European Conference on Networks and Communications (EuCNC)*. 2017, pp. 1–5. DOI: 10.1109/EuCNC.2017.7980743.

[4] R.V. Siva Balan, S. Deepa, and C. Balakrishnan. "Transforming towards 6G: Critical Review of Key Performance Indicators". In: *2022 4th International Conference on Circuits, Control, Communication and Computing (I4C)*. 2022, pp. 341–346. DOI: 10.1109/I4C57141.2022.10057812.

[5] Pieter Barnard et al. "Resource Reservation in Sliced Networks: An Explainable Artificial Intelligence (XAI) Approach". In: *ICC 2022 - IEEE International Conference on Communications*. 2022, pp. 1530–1535. DOI: 10.1109/ICC45855.2022.9838766.

[6] Bouziane Brik et al. *A Survey on Explainable AI for 6G O-RAN: Architecture, Use Cases, Challenges and Research Directions*. 2023. arXiv: 2307.00319 [cs.NI].

[7] Sebastian Cammerer et al. "A Neural Receiver for 5G NR Multi-user MIMO". In: *arXiv preprint arXiv:2312.02601* (2023).

[8] Congmin Fan, Xiaojun Yuan, and Ying-Jun Zhang. "CNN-based signal detection for banded linear systems". In: *IEEE Transactions on Wireless Communications* 18.9 (2019), pp. 4394–4407.

[9] J. A. Fernandez et al. "Performance of the 802.11p Physical Layer in Vehicle-to-Vehicle Environments". In: *IEEE Transactions on Vehicular Technology* 61.1 (2012), pp. 3–14.

[10] A. K. Gizzini et al. "Deep Learning Based Channel Estimation Schemes for IEEE 802.11p Standard". In: *IEEE Access* 8 (2020), pp. 113751–113765.

[11] Abdul Karim Gizzini and Marwa Chafii. "A Survey on Deep Learning Based Channel Estimation in Doubly Dispersive Environments". In: *IEEE Access* 10 (2022), pp. 70595–70619. DOI: 10.1109/ACCESS.2022.3188111.

[12] Abdul Karim Gizzini and Marwa Chafii. "Low Complex Methods for Robust Channel Estimation in Doubly Dispersive Environments". In: *IEEE Access* 10 (2022), pp. 34321–34339. DOI: 10.1109/ACCESS.2022.3162928.

[13] Abdul Karim Gizzini et al. *Explainable AI for Enhancing Efficiency of DL-based Channel Estimation*. 2024. arXiv: 2407.07009 [cs.AI]. URL: https://arxiv.org/abs/2407.07009.

[14] Abdul Karim Gizzini et al. "Joint TRFI and Deep Learning for Vehicular Channel Estimation". In: *IEEE GLOBECOM 2020*. Taipei, Taiwan, Dec. 2020.

[15] Abdul Karim Gizzini et al. "Towards Explainable AI for Channel Estimation in Wireless Communications". In: *IEEE Transactions on Vehicular Technology* (2023), pp. 1–6. DOI: 10.1109/TVT.2023.3345632.

[16] Mathieu Goutay et al. "End-to-end learning of OFDM waveforms with PAPR and ACLR constraints". In: *2021 IEEE Globecom Workshops (GC Wkshps)*. IEEE. 2021, pp. 1–6.

[17] Weisi Guo. "Explainable Artificial Intelligence for 6G: Improving Trust between Human and Machine". In: *IEEE Communications Magazine* 58.6 (2020), pp. 39–45. DOI: 10.1109/MCOM.001.2000050.

[18] S. Han, Y. Oh, and C. Song. "A Deep Learning Based Channel Estimation Scheme for IEEE 802.11p Systems". In: *IEEE International Conference on Communications (ICC)*. 2019, pp. 1–6.

[19] Mikko Honkala, Dani Korpi, and Janne MJ Huttunen. "DeepRx: Fully convolutional deep learning receiver". In: *IEEE Transactions on Wireless Communications* 20.6 (2021), pp. 3925–3940.

[20] Hongji Huang et al. "Deep Learning for Physical-Layer 5G Wireless Techniques: Opportunities, Challenges and Solutions". In: *IEEE Wireless Communications* 27.1 (2020), pp. 214–222. DOI: 10.1109/MWC.2019.1900027.

[21] Senthil Kumar Jagatheesaperumal et al. "Explainable AI Over the Internet of Things (IoT): Overview, State-of-the-Art and Future Directions". In: *IEEE Open Journal of the Communications Society* 3 (2022), pp. 2106–2136. DOI: 10.1109/OJCOMS.2022.3215676.

[22] Davinder Kaur et al. "Trustworthy Explainability Acceptance: A New Metric to Measure the Trustworthiness of Interpretable AI Medical Diagnostic Systems". In: *Complex, Intelligent and Software Intensive Systems*. Ed. by Leonard Barolli, Kangbin Yim, and Tomoya Enokido. Cham: Springer International Publishing, 2021, pp. 35–46. ISBN: 978-3-030-79725-6.

[23] Nasir Khan et al. “Explainable and Robust Artificial Intelligence for Trustworthy Resource Management in 6G Networks”. In: *IEEE Communications Magazine* (2023), pp. 1–7. DOI: 10.1109/MCOM.001.2300172.

[24] Guangyi Liu et al. “Vision, requirements and network architecture of 6G mobile network beyond 2030”. In: *China Communications* 17.9 (2020), pp. 92–104. DOI: 10.23919/JCC.2020.09.008.

[25] Scott M Lundberg and Su-In Lee. “A unified approach to interpreting model predictions”. In: *Advances in neural information processing systems* 30 (2017).

[26] X. Ma, H. Ye, and Y. Li. “Learning Assisted Estimation for Time- Varying Channels”. In: *2018 15th International Symposium on Wireless Communication Systems (ISWCS)*. 2018, pp. 1–5. DOI: 10.1109/ISWCS.2018.8491068.

[27] Alexandru-Daniel Marcu et al. “Explainable Artificial Intelligence for Energy-Efficient Radio Resource Management”. In: *2023 IEEE Wireless Communications and Networking Conference (WCNC)*. 2023, pp. 1–6. DOI: 10.1109/WCNC55385.2023.10119130.

[28] Timothy J O’Shea et al. “Radio transformer networks: Attention models for learning to synchronize in wireless systems”. In: *2016 50th Asilomar Conference on Signals, Systems and Computers*. IEEE. 2016, pp. 662–666.

[29] T. O’Shea and J. Hoydis. “An Introduction to Deep Learning for the Physical Layer”. In: *IEEE Transactions on Cognitive Communications and Networking* 3.4 (2017), pp. 563–575. DOI: 10.1109/TCCN.2017.2758370.

[30] Timothy J O’Shea, Johnathan Corgan, and T Charles Clancy. “Convolutional radio modulation recognition networks”. In: *Engineering Applications of Neural Networks: 17th International Conference, EANN 2016, Aberdeen, UK, September 2-5, 2016, Proceedings 17*. Springer. 2016, pp. 213–226.

[31] Ziyou Ren et al. “Sigt: An efficient end-to-end MIMO-OFDM receiver framework based on transformer”. In: *2022 5th International Conference on Communications, Signal Processing, and their Applications (ICCSPA)*. IEEE. 2022, pp. 1–6.

[32] Marco Tulio Ribeiro, Sameer Singh, and Carlos Guestrin. “" Why should i trust you?" Explaining the predictions of any classifier”. In: *Proceedings of the 22nd ACM SIGKDD international conference on knowledge discovery and data mining*. 2016, pp. 1135–1144.

[33] I. Sen and D. W. Matolak. “Vehicle–Vehicle Channel Models for the 5-GHz Band”. In: *IEEE Transactions on Intelligent Transportation Systems* 9.2 (2008), pp. 235–245.

[34] Cheng-Xiang Wang et al. “On the Road to 6G: Visions, Requirements, Key Technologies, and Testbeds”. In: *IEEE Communications Surveys & Tutorials* 25.2 (2023), pp. 905–974. DOI: 10.1109/COMST.2023.3249835.

[35] Yulei Wu, Guozhi Lin, and Jingguo Ge. “Knowledge-Powered Explainable Artificial Intelligence for Network Automation toward 6G”. In: *IEEE Network* 36.3 (2022), pp. 16–23. DOI: 10.1109/MNET.005.2100541.

[36] Helin Yang et al. “Artificial-Intelligence-Enabled Intelligent 6G Networks”. In: *IEEE Network* 34.6 (2020), pp. 272–280. DOI: 10.1109/MNET.011.2000195.

[37] Y. Yang et al. “Deep Learning-Based Channel Estimation for Doubly Selective Fading Channels”. In: *IEEE Access* 7 (2019), pp. 36579–36589. DOI: 10.1109/ACCESS.2019.2901066.

[38] Hao Ye, Geoffrey Ye Li, and Biing-Hwang Juang. “Power of deep learning for channel estimation and signal detection in OFDM systems”. In: *IEEE Wireless Communications Letters* 7.1 (2017), pp. 114–117.

[39] Yoon-Kyeong Kim et al. “Time and Frequency Domain Channel Estimation Scheme for IEEE 802.11p”. In: *17th International IEEE Conference on Intelligent Transportation Systems (ITSC)*. 2014, pp. 1085–1090.

[40] Shangwei Zhang et al. “Deep learning techniques for advancing 6G communications in the physical layer”. In: *IEEE Wireless Communications* 28.5 (2021), pp. 141–147.

[41] Zhongyuan Zhao et al. “Deep-waveform: A learned OFDM receiver based on deep complex-valued convolutional networks”. In: *IEEE Journal on Selected Areas in Communications* 39.8 (2021), pp. 2407–2420.

[42] Maede Zolanvari et al. “TRUST XAI: Model-Agnostic Explanations for AI With a Case Study on IIoT Security”. In: *IEEE Internet of Things Journal* 10.4 (2023), pp. 2967–2978. DOI: 10.1109/JIOT.2021.3122019.